

A low-cost method of fabricating hybrid micro-nano fluidic chip by double-layer PDMS mold and UV–thermal nanoimprinting

Lei Sun¹ · Zhifu Yin¹ · Liping Qi² · Dongjiang Wu³ · Helin Zou^{1,3}

Received: 24 November 2015 / Published online: 19 March 2016
© Springer-Verlag Berlin Heidelberg 2016

Abstract Micro-nano fluidic chips have become important tools in biomedical testing and research, their more frequent and diverse application being hampered mainly by their high cost, reflective of complex and expensive production methods. Our study introduces a simple, cost-effective new procedure whereby a sturdy PDMS mold consisting of two layers of poured PDMS with a photomask film bonded between them is used for replicating a hybrid micro-nano structure on a SU-8 substrate. The bottom surface of the mold receives a pattern of nano-ridges by pouring the first layer of PDMS on a 2D silicon nano-mold obtained by plasma etching after inclined Cu deposition. Using the double-layer PDMS mold, nano-channels can be imprinted with micro-channels cross-linked through the photomask in a single step of UV–thermal imprinting. The advantages of our end product, a chip with 205- μm -wide and 10- μm -deep micro-channels, cross-linked with 158-nm-wide and 90-nm-deep nano-channels, are its high precision and low cost.

Keywords Hybrid micro-nano channel · PDMS · Surface modification · UV–thermal nanoimprint

1 Introduction

With the increasing sophistication of micro-nano fabrication technology, microfluidic and nanofluidic chips have become established as tools in biomedical studies. Required for many applications are, however, not single-scale micro- or nano-devices, but multifunctional hybrid chips that combine nano- with micro-channels. One important application of these hybrid micro-nano devices is the detection and identification of biological macromolecules, such as DNA, by stringing them out in a single-molecule line (Mannion et al. 2006; Freedman et al. 2013). Much research has already been conducted to devise the methods of fabricating hybrid micro-nano devices. The different methods so far developed can be classified as follows:

1. Engraving by electron beam (EB) (Nam et al. 2010; Evstrapov et al. 2012), proton beam (PB) (Shao et al. 2007; Van Kan et al. 2011), focused ion beam (FIB) (Fanzio et al. 2011; Lopez-Bosque et al. 2013), or direct laser writing (Liao et al. 2013; Becker et al. 2013) are straightforward methods. However, these methods do not lend themselves to mass production because they are very costly and time-consuming.
2. Some researchers have transferred hybrid micro-nano structures directly from a silicon mold into a polymer substrate by thermal nanoimprint technology (Thamdrup et al. 2008; Carlberg et al. 2008; 2010). However, when nano-structures are next to the micro-structures on the mold, the polymer first fills the micro-structures and then fills the nano-structures. Due to stress relaxation of the viscoelastic polymer in the thermal nanoimprinting process, the inner stress of the polymer gradually decreases as time extending. Therefore, the

✉ Helin Zou
zouhl@dlut.edu.cn

¹ Key Laboratory for Precision and Non-traditional Machining Technology of Ministry of Education, Dalian University of Technology, Dalian, China

² Department of Biomedical Engineering, Dalian University of Technology, Dalian, China

³ Key Laboratory for Micro/Nano Technology and Systems of Liaoning Province, Dalian University of Technology, Dalian, China

polymer cannot reach the center of the nano-structures due to worse fluidity caused by low inner stress. This serious proximity effect will greatly reduce the replication accuracy of the patterns (Cheng and Guo 2004). To avoid the proximity effect, researchers (Okuda et al. 2007; Li et al. 2010) fabricated hybrid micro-nano channels by combination of the thermal and ultraviolet (UV) nanoimprinting, whereby the micro-channels are developed and the nano-channels are imprinted on the substrate. However, this method is of limited use because of the complicated and expensive fabrication of the hybrid quartz molds. In addition, quartz molds are not suitable for the manufacture of large-area hybrid micro-nano structures because of their high roughness and difficult demolding. Some researchers (Parka et al. 2010) improved the method by using a PDMS mold to make nano-structures on AMO-NIL layer and a quartz mask to make micro-structures on SU-8 layer, respectively, which is efficient and convenient. But the alignment between nano-patterns and micro-patterns is not easy.

- Recently, a number of researchers have fabricated hybrid micro-nano structures by casting PDMS (Van Kan et al. 2012; Liu et al. 2013; Hu et al. 2014). Van Kan et al. (2012) manufactured a silicon nano-mold by proton beam writing and then superimposed SU-8 micro-structures on it to create a hybrid micro-nano mold. Liu et al. (2013) made a hybrid nickel micro-nano mold by proton beam writing and etching technology. Hu et al. (2014) fabricated a hybrid silicon micro-nano silicon mold by AFM thermal writing and etching technology. In all these cases, the hybrid micro-nano structures were transferred from the mold into PDMS by casting. These methods can achieve

high-precision hybrid micro-nano structures, but the fabrication of the mold requires expensive equipment.

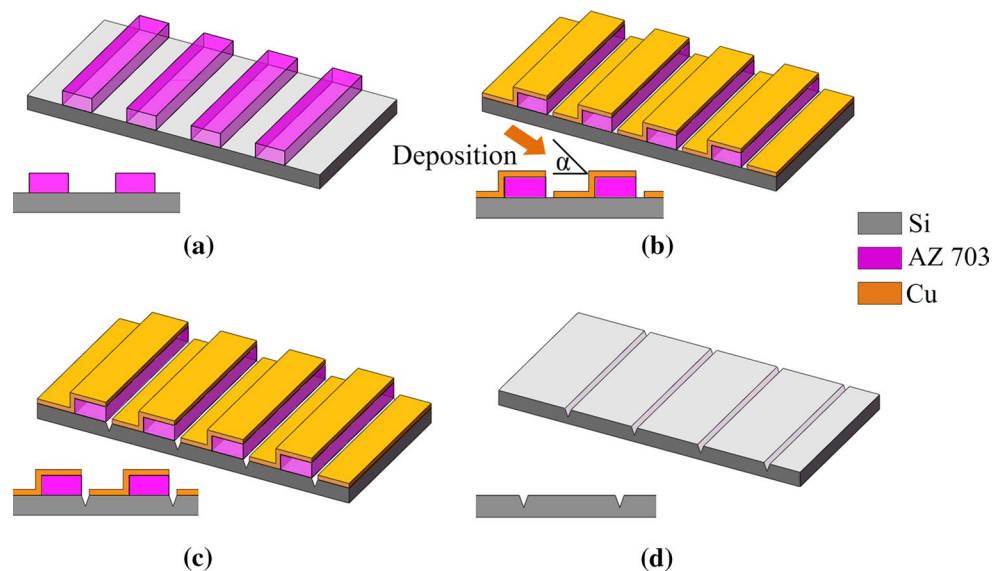
In this paper, we are introducing a novel cost-saving method of fabricating hybrid micro-nano channels. To avoid using expensive equipment (such as EB, PB and FIB), a 2D silicon nano-mold with the corresponding nano-channels, those having been inscribed by plasma etching after inclined Cu deposition over the substrate patterned with positive photoresist mesas, is used to fabricate double-layer (DL) PDMS mold. The bottom surface of the DL PDMS mold is given a pattern of nano-ridges by pouring the first layer of PDMS on the 2D silicon nano-mold, and a photomask film with micro-patterns is sandwiched between the first and the second layer of PDMS. The DL PDMS mold is easier to be fabricated rather than etching a quartz mold. The finished DL PDMS mold is then used to replicate the hybrid micro-nano channels into the SU-8 substrate by UV-thermal imprinting, the nano-channels by thermal imprinting, and the micro-channels by developing the negative photoresist. Compared to a quartz mold, the DL PDMS mold is flatter and easier to demold from the SU-8 photoresist, which improves the precision of the nano-patterns. This simple, low-cost manufacturing process can thus be used for mass-producing large-surface hybrid micro-nano channels.

2 Experiments

2.1 Fabrication of 2D silicon nano-mold

Figure 1a shows the silicon substrate with a micro-pattern of photoresist mesas. These mesas are what remained after

Fig. 1 Steps in the fabrication of the 2D silicon nano-mold: **a** micro-pattern of photoresist mesas on silicon substrate, **b** mesas and substrate covered with Cu film, **c** nano-channels etched in the silicon substrate, and **d** silicon substrate with nano-channels after removal of Cu and photoresist



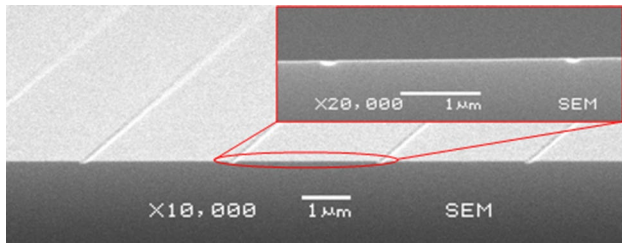


Fig. 2 SEM images of 2D silicon nano-mold

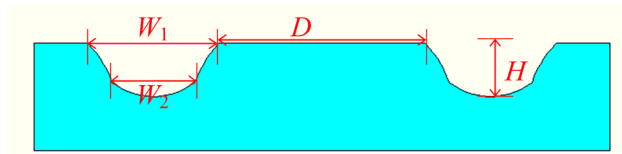


Fig. 3 Schematic diagram listing the dimensions of the 2D silicon nano-mold (H height of nano-channel, W_1 width measured at top of nano-channel, W_2 width measured at $0.9 \times H$ of nano-channel, D distance between adjacent nano-channels)

developing a 700-nm layer of positive photoresist (Shipley AZ 703), spin-coated at a speed of 7000 rpm for 30 s and exposed to UV light through a micro-pattern photomask. Figure 1b shows the silicon substrate and mesas covered with a Cu film that has been deposited for 30 min under an angle of $\alpha = 45.84^\circ$ in a thermal metal deposition system (ZZS400, Costar Group, China). Nano-sized gaps without Cu film formed through the shadow effect on the lee side along the base of each photoresist mesa. Then argon plasma etching was performed in a thin-film deposition

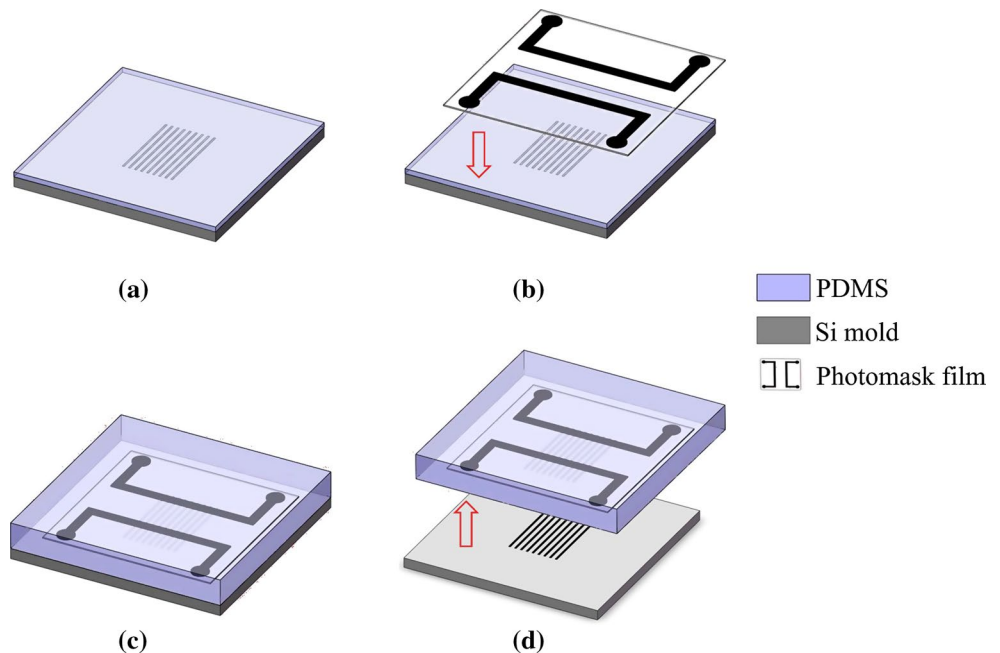
system (Kurt J. Lesker LAB18, France) under these parameters: chamber power of 100 W, argon pressure of 5 mtorr, and etching time of 30 min. During this process, etching of the silicon substrate occurred along the nano-sized gaps in the Cu mask at the foot of each mesa, as shown in Fig. 1c. The 2D silicon nano-mold, finished by removing the Cu and photoresist in boiling aqua regia ($\text{HCl}:\text{HNO}_3 = 3:1$), is shown in Fig. 1d.

Figure 2 shows the scanning electron microscopy (SEM) (JPS6360, Japan) images of the fabricated 2D silicon nano-mold. Dimensions of the nano-channel patterns are shown schematically in Fig. 3: height = H ; width = $W = (W_1 + W_2)/2$, where W_1 is the top width and W_2 is the width at $0.9 \times H$; distance between two adjacent nano-channels = D . The dimensions sizes of the 2D silicon nano-mold measured by the software named Smile View supplied by the SEM manufacturer (JEOL, Japan) are: $W_{\text{Si-mold}} = 146 \pm 5 \text{ nm}$, $H_{\text{Si-mold}} = 85 \pm 5 \text{ nm}$, $D_{\text{Si-mold}} = 3.00 \pm 0.01 \mu\text{m}$. The silicon nano-mold was then used to fabricate a double-layer PDMS mold, and the nano-channels were transformed into nano-ridges.

2.2 Fabrication of double-layer PDMS mold

As shown in Fig. 4a, the silicon nano-mold was treated by trimethyl chlorosilane (TMCS, $(\text{CH}_3)_3\text{SiCl}$) for 1 h, and then 3 ml uncured polydimethylsiloxane (PDMS, Dow Corning 184, base/curing agent = 5:1) was poured on top of it. The silicon nano-mold covered with PDMS was placed in a vacuum under 10 Pa for 30 min to remove bubbles and completely fill the nano-channels with PDMS. After baking at 60°C for 120 min, a continuous 500- μm -thick PDMS

Fig. 4 Double-layer PDMS mold fabrication process flow, **a** pour the first PDMS layer on the silicon nano-mold, **b** put photomask film on top surface of the first PDMS layer, **c** pour the second PDMS layer on the photomask film, and **d** detach the silicon nano-mold



layer was formed covering the silicon nano-mold. To add micro-structures into the PDMS mold, a photomask film with micro-patterns was put on top surface of the PDMS as shown in Fig. 4b and the parallel nano-structures were intersected by the micro-patterns. The first PDMS layer was too thin to demold from the silicon nano-mold, so a second PDMS layer was poured above the photomask. As shown in Fig. 4c, 15 ml uncured PDMS was poured on top of the photomask film. After baking at 60 °C for 120 min, a second layer of PDMS was formed to fix the photomask film. After removing the silicon nano-mold carefully with tweezers, the double-layer (DL) PDMS mold was successfully prepared, as shown in Fig. 4d. Using this method, the micro-photomask film and the nano-ridges are integrated in the DL PDMS mold. The high UV transmittance of PDMS makes the DL PDMS mold possible to be used for fabricating hybrid micro-nano channels by UV–thermal nano-imprinting, and the thin bottom PDMS layer leads to nearly contact exposure to SU-8 photoresist.

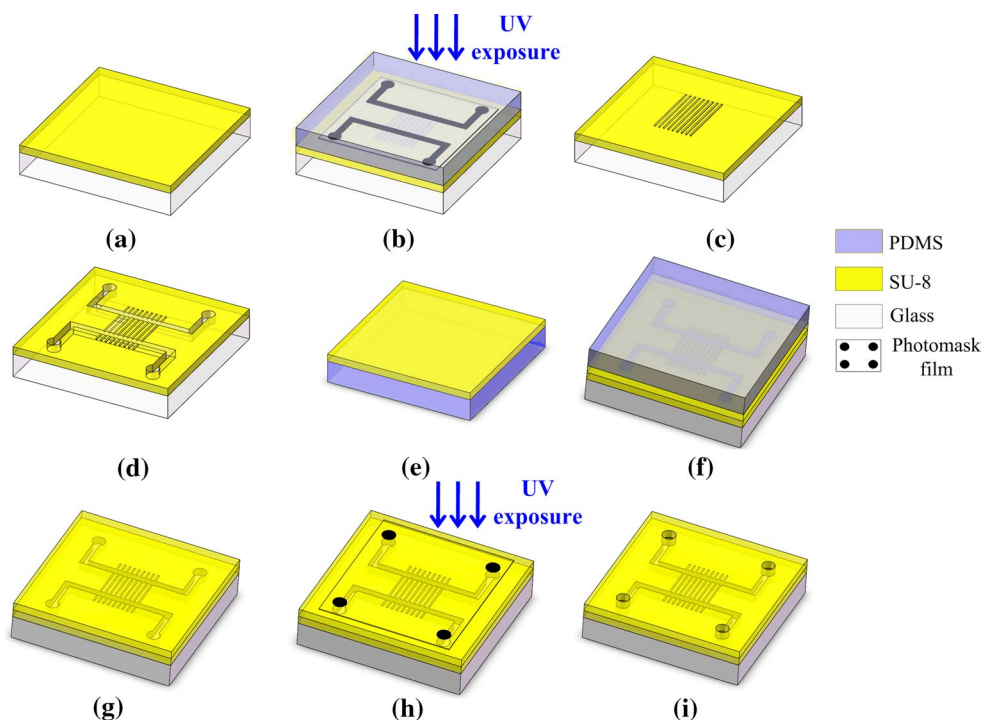
2.3 Fabrication of hybrid micro-nano fluidic chip

As shown in Fig. 5a, 15- μm -thick layer of SU-8 (Micro-Chem, SU-8 2015) was spin-coated on the glass substrate (1.5 cm \times 2.5 cm) at a speed of 4000 rpm for 30 s, followed by a prebake at 85 °C for 30 min to completely evaporate the solvent. Then, the glass substrate with prebaked SU-8 and the DL PDMS mold were pressed at 0.1 Mpa by two

clamps, and both of them were placed in a baking oven for hot embossing at 85 °C for 12 min. After cooling to room temperature, they were exposed to UV light at a dose of 1.4 mW/cm² for 12 min (exposure machine BGJ-3, China), the photomask film shielding the areas from exposure that were to form the intersecting micro-channels, as shown in Fig. 5b. After a postbake at 85 °C for 3 min, the DL PDMS mold was lifted off the SU-8 layer and all the unexposed SU-8 was developed in SU-8 developer for 30 s to form the micro-channels, as shown in Fig. 5c, d. That completed the fabrication of the hybrid micro-nano channels.

A 15- μm -thick layer of SU-8 was spin-coated on a PDMS at a speed of 4000 rpm for 30 s, followed by a prebake at 85 °C for 30 min to get a cover SU-8 layer, as shown in Fig. 5e. To improve the adhesion between two SU-8 layers, the patterned SU-8 layer and the cover SU-8 layer were treated with O₂ plasma (Emitech K1050X) under the parameters: 30 s at a chamber power of 30 W. Then, the two SU-8 layers were pressed at 0.05 Mpa by two clamps in a baking oven for thermal bonding at 50 °C for 5 min, as shown in Fig. 5f. After cooled to room temperature, the PDMS was carefully removed from the cover SU-8 layer, forming the sealed hybrid micro-nano channels, as shown in Fig. 5g. To make reservoirs, the product was exposed to UV light with a photomask for 12 min, followed by a postbake at 85 °C for 3 min and development for 30 s, as shown in Fig. 5h, i. That completed the fabrication of the hybrid micro-nano fluidic chip.

Fig. 5 Hybrid micro-nano channels fabrication process flow, **a** spin-coat SU-8 photoresist on the glass, **b** UV–thermal nanoimprinting by using DL PDMS mold, **c** remove DL PDMS mold to form the nano-channels, **d** develop SU-8 photoresist to obtain micro-channels, **e** spin-coat SU-8 photoresist on the PDMS, **f** thermal bonded, **g** remove PDMS, **h** UV exposure, and **i** develop to obtain reservoirs



3 Results and discussion

3.1 Surface modification of the silicon nano-mold

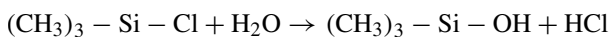
Before pouring the first PDMS layer (Fig. 2a), the silicon nano-mold was cleaned in boiling concentrated sulfuric acid. This process increases the surface energy of the silicon nano-mold through the formation of hydrophilic Si–OH groups. This high surface energy of the silicon nano-mold would make it difficult to separate from PDMS, and that would damage the nano-structures of the DL PDMS mold.

To achieve nondestructive demolding, the silicon nano-mold was treated with trimethyl chlorosilane (TMCS, $(\text{CH}_3)_3\text{SiCl}$) before pouring the PDMS. TMCS treatment was carried out in a drying tower jar, where the silicon nano-mold was placed for one hour so that TMCS vapor could adhere to its surface and react with the Si–OH groups to form $-\text{CH}_3$ groups (Wang Juan et al. 2004) as follows:



The deionized water contact angle of the silicon nano-mold surface was measured by the Drop Shape Analysis System (DSA100, Kruss Company, Germany). As shown in Fig. 6, the water contact angle of the silicon nano-mold was 34.2° before the treatment (Fig. 6a) increasing to 84.5° after the treatment (Fig. 6b).

However, longtime exposure to air after treatment will let the surface hydrophobicity of the silicon nano-mold deteriorate. As can be seen in Fig. 6c, 24 h after treatment with TMCS, the contact angle of the silicon nano-mold falls back to 70.4° . This is probably caused by the decay loss of the TMCS due to the reaction with aqueous vapor (Wang Juan et al. 2004) as follows:



These results indicate that the surface modification by TMCS is effective but temporal. Therefore, PDMS has to be poured on the surface of the silicon nano-mold immediately after TMCS treatment.

3.2 The influence of O_2 plasma treatment parameters on the contact angle of PDMS and the photomask film

Before pouring the second PDMS layer, the photomask film (PET, polyethylene terephthalate) was placed on the first PDMS layer, as shown in Fig. 4b. Because the low surface energy of PDMS keeps these two kinds of materials from making full contact with each other, bubbles tend to appear between the photomask film and the first PDMS layer, whose bottom plane will therefore be deformed after removing the silicon nano-mold. Besides, if the bonding strength between the PDMS layer and the photomask film is not strong enough, the DL PDMS mold will be broken where the photomask film was placed when detaching the DL PDMS mold from the SU-8 photoresist. To enable full contact and increase bonding strength between the first PDMS layer and the photomask film, both were treated with O_2 plasma (Emitech K1050X) to increase their surface energy before pouring the second PDMS layer. The influence of the chamber power and treatment time of the plasma etcher on the water contact angle of PDMS and photomask film is shown in Fig. 7, O_2 pressure being fixed at 7×10^{-1} mbar.

As shown in Fig. 7, at zero treatment time the water contact angle of native PDMS is 114.5° (Fig. 7a) and that of photomask film is 80.3° (Fig. 7b), with an expected decrease after treatment with O_2 plasma. That decrease levels out and reaches a practical limit after about 15 s for PDMS, and after 10–15 s for photomask film. For PDMS, as shown in Fig. 7a, the contact angle drops faster with a higher chamber power, and it falls below 10° as treatment time approaches 20 s, no matter whether the chamber power is 15 or 25 W. For photomask film, as shown in Fig. 7b, plasma etcher chamber power of either 15 or 25 W achieves an almost identical decrease. And after a 15 s treatment, the contact angle of photomask film levels out to about 35° , regardless of the difference in chamber power (5, 15, or 25 W).

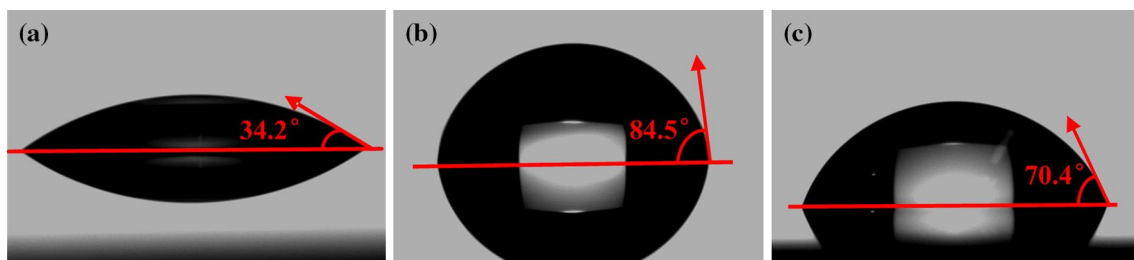


Fig. 6 Contact angle of the silicon nano-mold, **a** untreated, **b** treated with TMCS, and **c** 24 h after treatment with TMCS

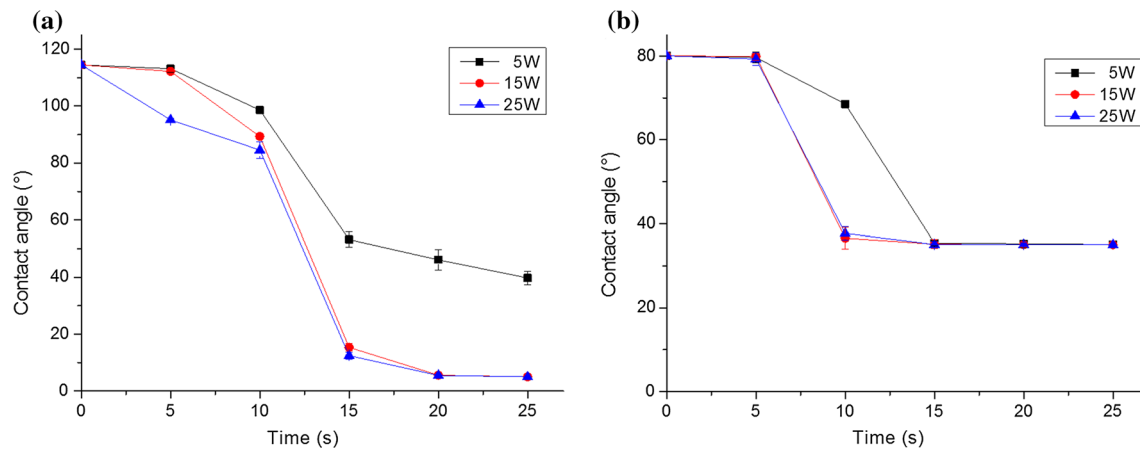


Fig. 7 Influence of chamber power and treatment time of the plasma etcher on the contact angle of PDMS and photomask film, **a** PDMS and **b** photomask film (O_2 pressure: 7×10^{-1} mbar)

As is well known, the smaller the water contact angle, the higher the bonding strength of PDMS and photomask film (Ozgen et al. 2013), and high-power O_2 plasma will etch both the photomask film and PDMS. Based on the results of our experiments, we chose a treatment time of 20 s and plasma etcher chamber power of 15 W as the optimal parameters for PDMS, while for photomask film the optimal parameters were determined to be a treatment time of 15 s and plasma etcher chamber power of 5 W.

3.3 Optimization of the exposure time during the UV lithography

In Fig. 5b, the micro-channels were shielded by the photomask of the DL PDMS mold, and the nano-channels were cross-linked by UV light. Therefore, the exposure time of UV light has great influence on the surface topography of both micro- and nano-channels. In order to fabricate high-precision hybrid micro-nano channels, the exposure time was optimized.

To optimize the time of exposure to UV light, its impact on the surface topography of micro-channels and nano-channels was investigated. Figure 8 shows the SEM

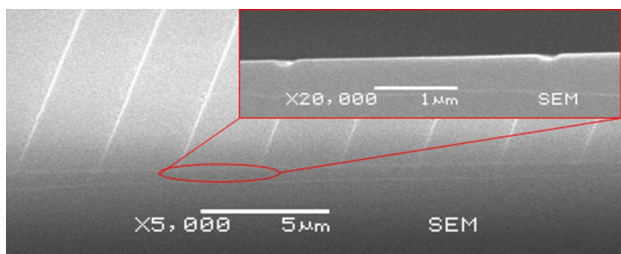


Fig. 8 SEM images of the SU-8 nano-channels by thermal imprint before developing ($W_{SU8} = 149 \pm 5$ nm, $H_{SU8} = 85 \pm 5$ nm)

images of the nano-channels by thermal imprint before developing, of which the size is: $W_{SU8} = 149 \pm 5$ nm $H_{SU8} = 85 \pm 5$ nm, as shown above in Fig. 3. Figures 9 and 10 then show the differences in micro- and nano-channel topography in the developed SU-8 layer after different UV exposure times.

Figure 9 shows the optical microscope (Olympus STM6, Japan) images of micro-channels and nano-channels at different exposure times. As shown in Fig. 9a, when the exposure time is shorter than 4 min, the SU-8 micro-structures are seriously damaged, since cross-linking in the SU-8 photoresist does not fully occur due to insufficient exposure. However, with the exposure time as long as 16 min, excessive cross-linking in the overexposed SU-8 photoresist leads to blocked micro-channels, as shown in Fig. 9d. Because SU-8 layer is not contacted to the photomask, during the process of UV exposure, interference of UV light occurs in the additional PDMS layer between the SU-8 photoresist and the photomask. When exposure dose is low, the interference UV light is weak and has a small effect on the micro-channels. But when exposure dose is high, the interference UV light is strong enough to expose the micro-channels, leading to the cross-linking in the SU-8 photoresist. Therefore, the micro-channels are blocked after development.

In Fig. 9b, c, when the exposure time is 8 and 12 min, both outlines of the micro-channels are clear, but the differences between those two nano-channels cannot be observed under the optical microscope. So we took the cross-section SEM images of the nano-channels exposed for 8 min and those exposed for 12 min to observe them in greater details. As shown in Fig. 10a, when the exposure time is 8 min, the size of the nano-channels ($W_{SU8-8 \text{ min}} = 237 \pm 5$ nm $H_{SU8-8 \text{ min}} = 93 \pm 3$ nm) is much larger than before developing (Fig. 8). This is probably because that SU-8 photoresist is

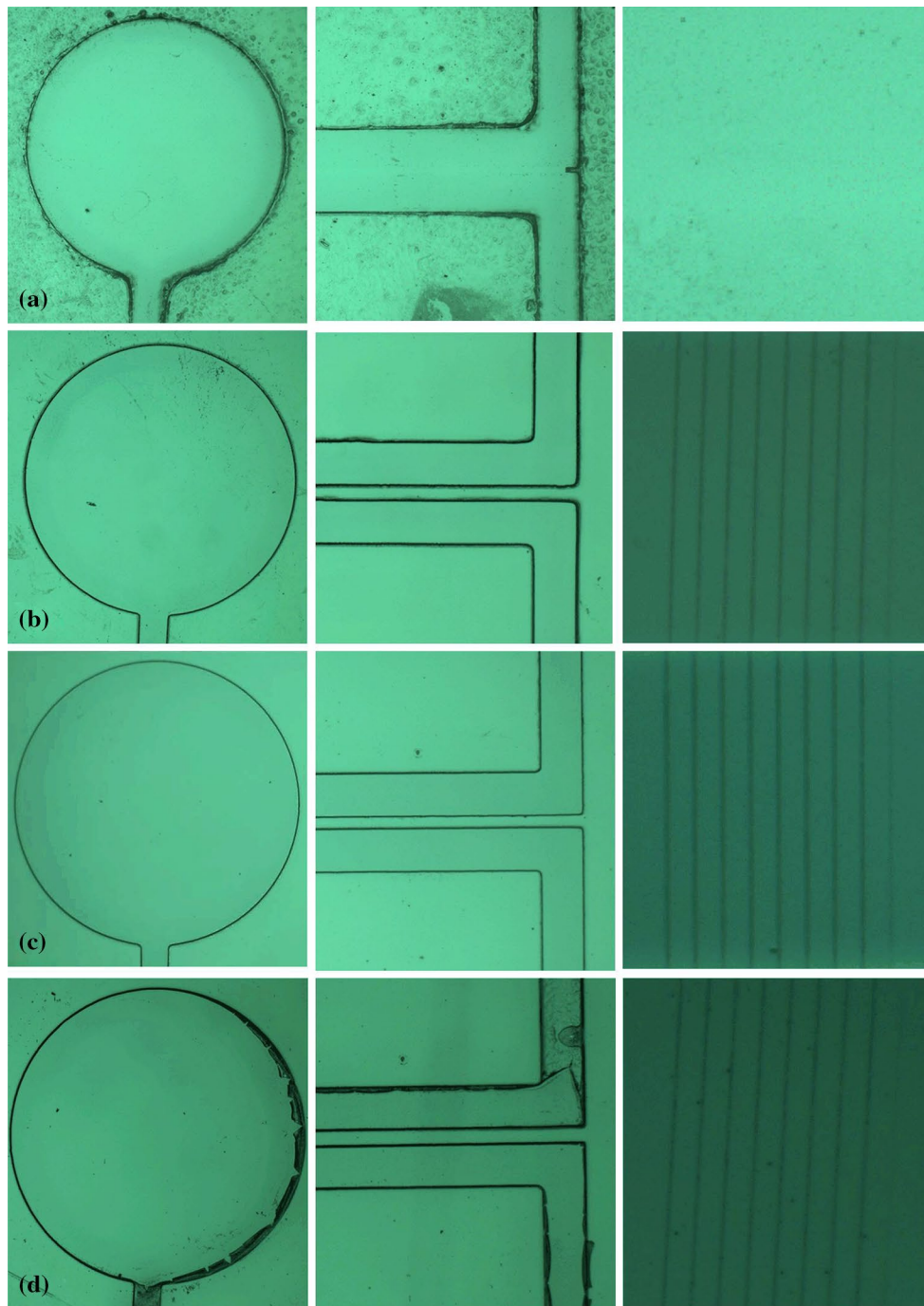


Fig. 9 Microscopic images of the SU-8 micro-channels and nano-channels developed after different exposure times (exposure intensity: 1.4 mw/cm^2), **a** 4 min, **b** 8 min, **c** 12 min, and **d** 16 min

underexposed, which causes insufficient concentration of photo-acid generator. After postbaking at $85 \text{ }^\circ\text{C}$ for 3 min, the nano-channels cannot be completely cross-linked due to a deficiency in cross-linking catalyst. During developing in SU-8 developer for 30 s, some nano-channels without being cross-linked were developed. However, at an exposure time of 12 min, the nano-channels were fully exposed

to be cross-linked. As shown in Fig. 10b, the nano-channels ($W_{\text{SU8-12 min}} = 159 \pm 7 \text{ nm}$, $H_{\text{SU8-12 min}} = 86 \pm 4 \text{ nm}$) were not corroded and of a higher replication precision. Therefore, the optimal exposure time for the SU-8 layer was determined to be 12 min.

The final hybrid micro-nano channels fabricated under optimal parameters are shown in Fig. 11. The dimensions of

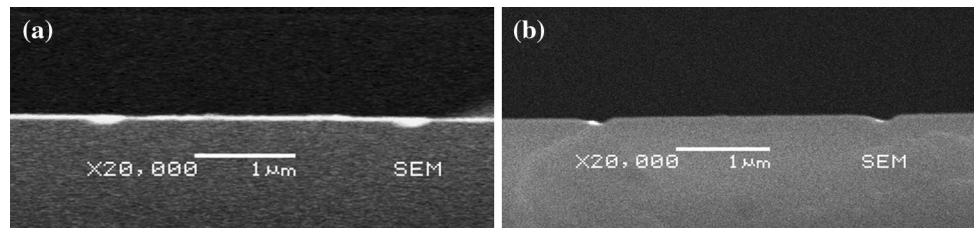


Fig. 10 Cross-section SEM images of the SU-8 nano-channels developed after different exposure times (exposure intensity: 1.4 mw/cm^2), **a** 8 min ($W_{\text{SU-8 min}} = 237 \pm 5 \text{ nm}$ $H_{\text{SU-8 min}} = 93 \pm 3 \text{ nm}$) and **b** 12 min ($W_{\text{SU-8-12 min}} = 159 \pm 7 \text{ nm}$ $H_{\text{SU-8-12 min}} = 86 \pm 4 \text{ nm}$)

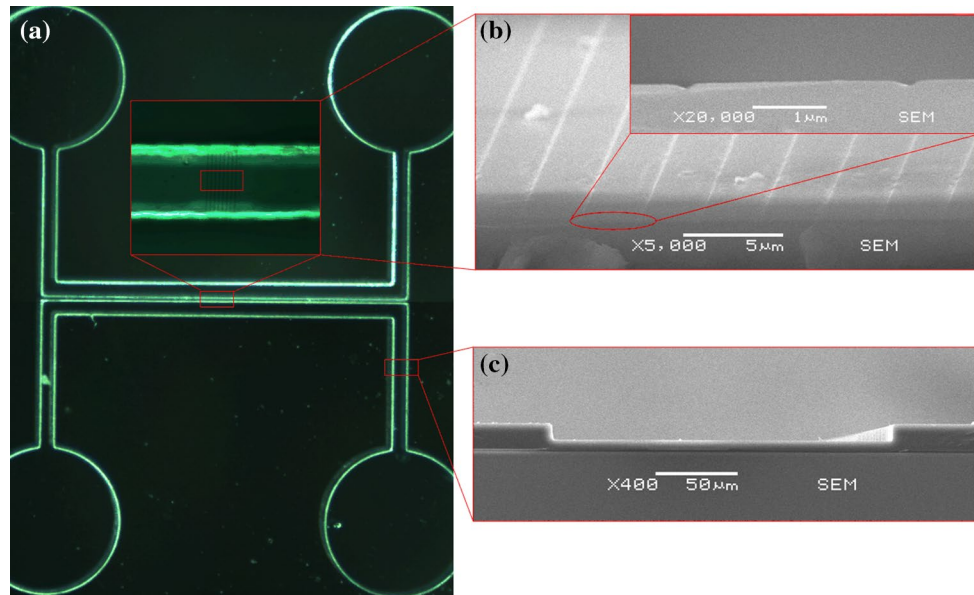


Fig. 11 Images of SU-8 hybrid structures, **a** plane view of hybrid patterns, **b** SEM images of SU-8 nano-channels ($W_{\text{nano}} = 159 \pm 7 \text{ nm}$ $H_{\text{nano}} = 86 \pm 4 \text{ nm}$), and **c** SEM image of SU-8 micro-channels ($W_{\text{micro}} = 205.0 \pm 0.2 \mu\text{m}$ $H_{\text{micro}} = 10.0 \pm 0.3 \mu\text{m}$)

the micro-channels are: $W_{\text{micro}} = 205.0 \pm 0.2 \mu\text{m}$ $H_{\text{micro}} = 10.0 \pm 0.3 \mu\text{m}$. The width of the micro-channels is $5\text{-}\mu\text{m}$ deviation from the photomask ($200 \mu\text{m}$). This is because the SU-8 photoresist is not contacted to the photomask, and the interference of UV light occurs in the additional PDMS layer between the SU-8 photoresist and the photomask during the process of UV exposure. Under the optimal exposure time, the interference UV light is weak and has a small effect on the micro-channels. The $5\text{-}\mu\text{m}$ deviation between the photomask and micro-channels has little influence on the whole structures. The dimensions of the nano-channels are: $W_{\text{nano}} = 159 \pm 7 \text{ nm}$ $H_{\text{nano}} = 86 \pm 4 \text{ nm}$. Compared against the silicon nano-mold in Fig. 2 ($W_{\text{Si-mold}} = 146 \pm 5 \text{ nm}$ $H_{\text{Si-mold}} = 85 \pm 5 \text{ nm}$), the replication errors for the nano-channels are: $\Delta W = W_{\text{nano}} - W_{\text{Si-mold}} = 13 \pm 12 \text{ nm}$ $\Delta H = H_{\text{nano}} - H_{\text{Si-mold}} = 1 \pm 9 \text{ nm}$. The results show that the replication precision of the nano-channels is very high. Furthermore, the DPL mold employed in this study was used for about 50 times without being damaged in any way.

3.4 Rhodamine dye filling test of bonded hybrid micro-nano channels

The hybrid micro-nano channels were sealed by thermal bonding at pressure of 0.05 MPa and time of 5 min . To fully bond the hybrid micro-nano channels without leakage and block, the different bonding temperature were chosen (45 , 50 , and $55 \text{ }^\circ\text{C}$). The profiles were observed by an optical microscope (Olympus STM6, Japan). As shown in Fig. 12a, when bonded under $45 \text{ }^\circ\text{C}$, the bubbles (unsealed areas) existed between the bonding surfaces, and the nano-channels were not fully sealed. However, when bonding temperature was $55 \text{ }^\circ\text{C}$, the SU-8 flowed into the nano-channels, and the nano-channels were blocked (Fig. 12c). Therefore, the bonding temperature was set at $50 \text{ }^\circ\text{C}$, so that the nano-channels can be fully sealed (Fig. 12b). Figure 13 is the cross-section SEM images of the nano-channels (SEM, Hitachi S-4800, Japan) and micro-channels (SEM, JPS6360, Japan) bonded under $50 \text{ }^\circ\text{C}$ for 5 min . The dimensions of

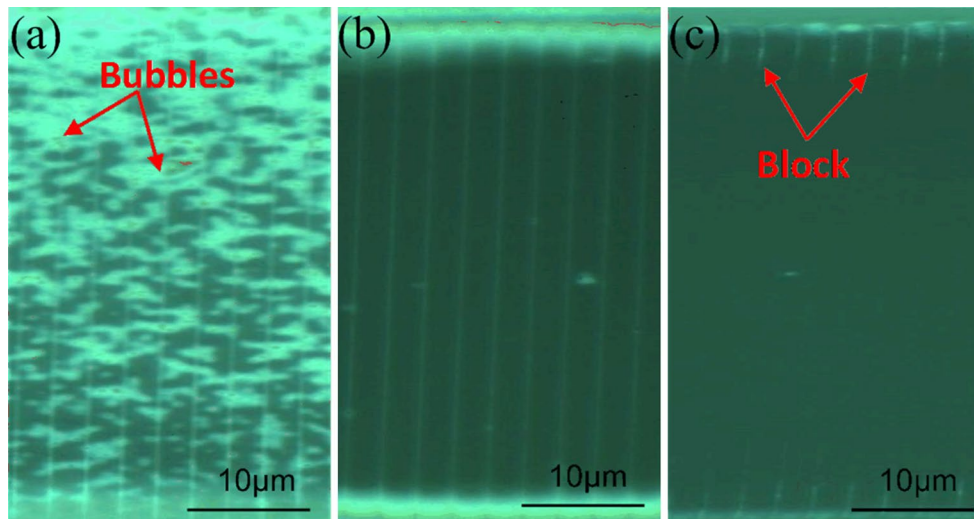


Fig. 12 Microscopic images of the bonded nano-channels, **a** bonded under 45 °C, **b** bonded under 50 °C, and **c** bonded under 55 °C (bonding pressure: 0.05 MPa, bonding time: 5 min)

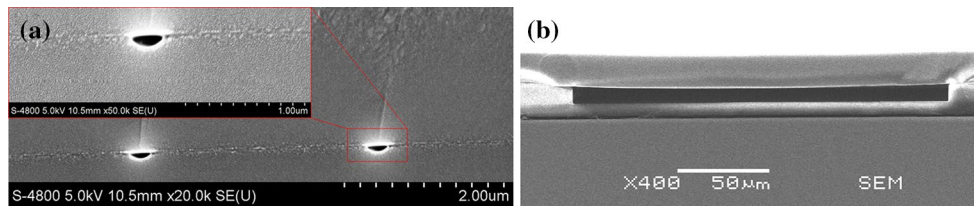


Fig. 13 SEM images of the hybrid micro-nano channels bonded under 50 °C for 5 min, **a** sealed nano-channels, and **b** sealed micro-channels

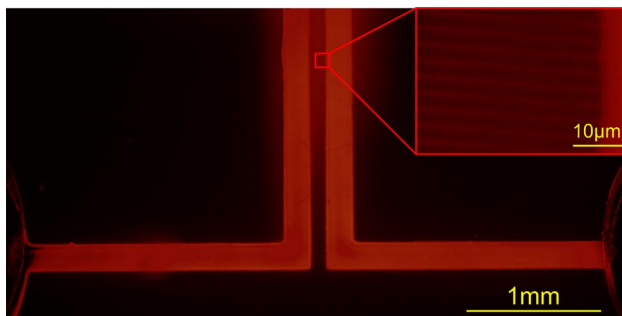


Fig. 14 Fluorescence image of the hybrid micro-nano fluidic chip filled with Rhodamine B solution

the bonded nano-channels are: $W_{\text{nano-bonded}} = 158 \pm 5 \text{ nm}$
 $H_{\text{nano-bonded}} = 90 \pm 5 \text{ nm}$. Compared against the nano-channels before bonded in Fig. 11 ($W_{\text{nano}} = 159 \pm 7 \text{ nm}$
 $H_{\text{nano}} = 86 \pm 4 \text{ nm}$), the errors for the nano-channels are: $\Delta W = W_{\text{nano-bonded}} - W_{\text{nano}} = -1 \pm 12 \text{ nm}$
 $\Delta H = H_{\text{nano-bonded}} - H_{\text{nano}} = 4 \pm 9 \text{ nm}$.

The hybrid micro-nano fluidic chip was tested by a fluorescent dye (20 mg/ml solution of Rhodamine B in absolute ethanol). The Rhodamine B dye could be excited and

observed by an inverted fluorescence microscope (Olympus IX71, Japan). As shown in Fig. 14, the fluorescent dye was filled into the sealed micro-channels and nano-channels by capillary force. The experimental results prove that the hybrid micro-nano channels can be bonded without blocking and leakage at temperature of 50 °C, pressure of 0.05 MPa, and time of 5 min. The hybrid micro-nano fluidic chip can be used for integrated photonics devices (Xie et al. 2008) and detection and immobilization of DNA (Yang et al. 2007; Brennan and Lambkin 2008; Erkan et al. 2008).

4 Conclusions

A low-cost hybrid micro-nano channels fabrication method was demonstrated in this paper. A 2D silicon nano-mold was fabricated by plasma etching after inclined Cu deposition and then used for making a double-layer (DL) PDMS mold consisting of two layers poured PDMS and a sandwiched photomask film with micro-patterns. To ensure the necessary adhesion between the first PDMS layer and the photomask film, both had to undergo an optimized

treatment with O₂ plasma: 20 s at a chamber power of 15 W in the case of the PDMS top surface, 15 s at a chamber power of 5 W for the photomask film. Optimized parameters were also determined for the UV–thermal micro-nano imprinting into the layer of SU-8: UV exposure time of 12 min with an exposure intensity of 1.4 mW/cm². Under these optimal parameters, high-precision hybrid devices with 205 μm wide by 10 μm deep micro-channels and 158 nm wide by 90 nm deep nano-channels were fabricated by using the DL PDMS mold. After thermal bonding at 0.05 MPa, 50 °C for 5 min, the hybrid micro-nano fluidic chip is characterized by Rhodamine dye filling test, which shows the availability of the device. This method has thus a high potential for mass production of hybrid micro-nano fluidic chips at low cost and with high replicating precision.

Acknowledgments This work was funded under National Natural Science Foundation of China (Project Numbers 91023046, 51075059) and Specialized Research Fund for the Doctoral Program of Higher Education (SRFDP).

References

- Becker H, Dewanda F, Ahsan MS, Lee MS, Gray BL (2013) Fabrication of micro/nano-fluidic channels by single-beam direct femtosecond laser writing. *Microelectron Eng* 87:722–725. doi:10.1117/12.2003347
- Brennan D, Lambkin P (2008) An integrated optofluidic platform for DNA hybridization and detection. *IEEE Sens J* 8:536–542. doi:10.1109/JSEN.2008.918963
- Carlberg P, Montelius L, Tegenfeldt J (2008) Nanoimprint in PDMS on glass with two-level hybrid stamp. *Microelectron Eng* 85:210–213. doi:10.1016/j.mee.2007.05.010
- Cheng X, Guo LJ (2004) One-step lithography for various size patterns with a hybrid mask-mold. *Microelectron Eng* 71:288–293. doi:10.1016/j.mee.2004.01.042
- Erkan Y, Halma K, Czolkos I, Jesorka A, Dommersnes P, Kumar R, Brown T, Orwar O (2008) Controlled release of CholTEG-DNA from nano- and micropatterned SU-8 surfaces by a spreading lipid film. *Nano Lett* 8:227–231. doi:10.1021/nl0725087
- Evstrapov AA, Mukhin IS, Bukatin AS, Kukhtevich IV (2012) Ion and electron beam assisted fabrication of nanostructures integrated in microfluidic chips. *Nucl Instrum Methods Phys Res Sect B* 282:145–148. doi:10.1016/j.nimb.2011.08.035
- Fanzio P, Mussi V, Manneschi C, Angeli E, Firpo G, Repetto L, Valbusa U (2011) DNA detection with a polymeric nano-channel device. *Lab Chip* 11:2961–2966. doi:10.1039/c1lc20243j
- Freedman KJ, Haq SR, Edel JB, Jemth P, Kim MJ (2013) Single molecule unfolding and stretching of protein domains inside a solid-state nanopore by electric field. *Sci Rep* 3:1638. doi:10.1038/srep01638
- Hu H, Zhuo Y, Oruc ME, Cunningham BT, King WP (2014) Nanofluidic channels of arbitrary shapes fabricated by tip-based nanofabrication. *Nanotechnology* 25:455301. doi:10.1088/0957-4484/25/45/455301
- Li X, Wang X, Jin J, Tang Q, Tian Y, Fu S, Cui Z (2010) Fabrication of micro/nano fluidic system combining hybrid mask-mould lithography with thermal bonding. *Microelectron Eng* 87:722–725. doi:10.1016/j.mee.2009.12.024
- Liao Y, Cheng Y, Liu C, Song J, He F, Shen Y, Chen D, Xu Z, Fan Z, Wei X, Sugioka K, Midorikawa K (2013) Direct laser writing of sub-50 nm nanofluidic channels buried in glass for three-dimensional micro-nanofluidic integration. *Lab Chip* 13:16–26. doi:10.1039/c3lc41171k
- Liu F, Tan KB, Malar P, Bikkarolla SK, van Kan JA (2013) Fabrication of nickel molds using proton beam writing for micro/nano fluidic devices. *Microelectron Eng* 102:36–39. doi:10.1016/j.mee.2012.05.020
- Lopez-Bosque MJ, Tejada-Montes E, Cazorla M, Linacero J, Atienza Y, Smith KH, Llado A, Colombelli J, Engel E, Mata A (2013) Fabrication of hierarchical micro-nanotopographies for cell attachment studies. *Nanotechnology* 24:255–305. doi:10.1088/0957-4484/24/25/255305
- Mannion JT, Reccius CH, Cross JD, Craighead HG (2006) Conformational analysis of single DNA molecules undergoing entropically induced motion in nanochannels. *Biophys J* 90:4538–4545. doi:10.1529/biophysj.105.074732
- Nam SW, Lee MH, Lee SH, Lee DJ, Rosnagel SM, Kim KB (2010) Sub-10-nm nanochannels by self-sealing and self-limiting atomic layer deposition. *Nano Lett* 10:3324–3329. doi:10.1021/nl100999e
- Okuda K, Niimi N, Kawata H, Hirai Y (2007) Micro-nano mixture patterning by thermal-UV novel nanoimprint. *J Vac Sci Technol B* 25:2370–2372. doi:10.1116/1.2801859
- Ozgen O, Aksoy EA, Hasirci V, Hasirci N (2013) Surface characterization and radical decay studies of oxygen plasma-treated PMMA films. *Surf Interface Anal* 45:844–853. doi:10.1002/sia.5181
- Parka S, Kimb G, Choib K, Lee J (2010) Fabrication of a 3D stamp with the micro- and nano-scale patterns through combined NIL and optical lithography processes. *Microelectron Eng* 87:968–971. doi:10.1016/j.mee.2009.11.132
- Shao PG, van Kan JA, Wang LP, Ansari K, Bettiol AA, Watt F (2007) Rapid prototyping of micro/nano poly (methyl methacrylate) fluidic systems using proton beam writing. *Nucl Instrum Methods Phys Res Sect B* 260:362–365. doi:10.1016/j.nimb.2007.02.047
- Thamdrup LH, Klukowska A, Kristensen A (2008) Stretching DNA in polymer nanochannels fabricated by thermal imprint in PMMA. *Nanotechnology* 19:125301. doi:10.1088/0957-4484/19/12/125301
- Thamdrup LH, Larsen NB, Kristensen A (2010) Light-induced local heating for thermophoretic manipulation of DNA in polymer micro- and nanochannels. *Nano Lett* 10:826–832. doi:10.1021/nl903190q
- Van Kan JA, Shao PG, Wang YH, Malar P (2011) Proton beam writing a platform technology for high quality three-dimensional metal mold fabrication for nanofluidic applications. *Microsyst Technol* 17:1519–1527. doi:10.1007/s00542-011-1321-z
- Van Kan JA, Zhang C, Perumal Malar P, van der Maarel JR (2012) High throughput fabrication of disposable nanofluidic lab-on-chip devices for single molecule studies. *Biomicrofluidics* 6:36502. doi:10.1063/1.4740231
- Wang J, Zhang CR, Feng J (2004) Modification of Nanoporous Silica Film By Trimethylchlorosilane. *Acta Phys Chim Sin* 20:1399–1403. doi:10.3866/PKU.WHXB20041201
- Xie S-Q, Wan J, Bing-Rui L, Sun Y, Chen Y, Qu X-P, Liu Ran (2008) A nanoimprint lithography for fabricating SU-8 gratings for near-infrared to deep-UV application. *Microelectron Eng* 85:914–917. doi:10.1016/j.mee.2008.01.072
- Yang B, Dukkipati VR, Li D, Cardozo BL, Pang SW (2007) Stretching and selective immobilization of DNA in SU-8 micro- and nanochannels. *J Vac Sci Technol B* 25:2352–2356. doi:10.1116/1.2806975